The Indian Geographical Journal
Volume 98 (1) June - 2023, pp 48-66
ISSN 0019-4824

MODELLING URBAN HEAT ISLAND USING REMOTE SENSING INDICES IN TIRUPPUR MUNICIPAL CORPORATION, TAMIL NADU

Masilamani Palanisamy, Prawin Balasubramaniam, Thilagaraj Periasamy

Department of Geography, Bharathidasan University, Tiruchirappalli,
Tamil Nadu, India - 620024.
Corresponding Author: masilamani@bdu.ac.in

Abstract

In the history of humankind, urbanization is one of the vibrant changing geographical phenomena. Almost 55% of the world's population lives in rapidly urban and surrounding areas. Urban heat island represents a significant environmental problem most urban centres face. Extreme heat in urban areas reflects substantial risks to the growing urban population. The increased surface temperature is due to the thermodynamic characteristics of the built-up in urban. The impact of land use/land cover (LULC) dynamics is closely related to urban heat islands (UHI). This study aims to identify the urban heat zones by utilising indicators such as the LULC, NDBI, LST and NDVI for Tiruppur Corporation. The study area Tiruppur is known as the knitwear capital of India, attracting thousands of migrants from all over the country and leading to a continuous accumulation of people. So, most of the migrant people settled in the Tiruppur belt. The present study analysed the spatio-temporal land-use patterns, NDBI, LST, NDVI and UTFVI for Tiruppur Corporation using Landsat and sentinel data sets for 1991, 2001, 2011 and 2021. The LULC were prepared by utilising the supervised classification algorithm of Support Vector Machine (SVM). On the other hand, the advanced technique of Google Earth Engine is utilised to map the LST and NDVI of the study area for the same year. All the results of four indicators, i.e., LULC, NDBI, LST, NDVI and UTFVI, are analysed with the temporal changes by segmenting them with six rings of each 2km. This will help to identify the changes and increase of urban heat from the core to the periphery areas of the Tiruppur Corporation. Thus, this study aids in improving future urban planning, including implementing green city technologies.

Keywords LULC, Tiruppur Corporation, LST, UHI, UTFVI.

Introduction

In recent decades, migration from rural to urban areas has drastically increased due to several factors (employment, education, economy, etc.), which has led to rapid urbanization and urban population growth (Kesavan et al., 2021). In 2016, the urban population reached 54.5% globally; if this continues, the urban population will be 60% of the

total world population by 2030 (U.N. 2016). This growth will convert the historical land use /land cover (LULC) pattern, which impacts the environmental and economic perspectives (Wang et al., 2018; Prakash et al., 2023). The change in LULC would cause changes not only in the landscape but also in the atmospheric conditions of the urban environment, such as the urban heat island (UHI) effect. The effect of the increased surface temperature in urban areas determines UHI (Weng et al. 2004). The growth of the impermeable surface and the decrease in the green space and water bodies are the leading causes of the temperature variation between urban and rural landscapes (Ranagalage et al., 2018). The growth of the city and its population are the indirect indicators of the UHI (Zhao et al. 2014); likewise, buildings, the nature of surfaces, including albedo, and heat capacity largely influence the UHI phenomena.

Highly populated countries like India and China are projected to occupy 35% of the total world urban population by the year 2050 (Bongaarts 2020). The UHI shows severe effects in these rapidly urbanizing countries (Peng et al., 2021). Hence, intensive research on diversified urban settings is needed to address the impacts of UHI (Zhou et al. 2019). The impacts of UHI are assessed through remote sensing (RS), vertical sensing, fixed stations, mobile traverses (Brandsma and Wolters 2012), and energy balances. Among these techniques, remote sensing is a more advanced and feasible method to measure both the air and surface temperature. The traditional methods like fixed station and mobile traverse are expensive and time-consuming (Padmanaban et al. 2017). The combination of remote sensing and Geographical Information System (GIS) techniques is considered to be the best method for observing environmental changes (Xiao et al., 2020). However, spatial and temporal resolution in remote sensing are the constraints in UHI assessments.

According to Weng et al. (2004), Land surface temperature (LST) is a fundamental indicator in UHI studies due to its capability to map temperature differences within urban areas, helping to pinpoint hotspots and assess their spatial extent. LST is the temperature measured on the earth's surface between land and atmosphere (Stow and Chen 2002). The changes in LULC play a significant role in the LST increase in the urban centres. The spatiotemporal changes of the LULC can be monitored using RS and GIS (Abdikan et al. 2014). The temporal LULC changes help to understand the land use types transformation, and it provides information about urban planning (Gordon et al. 2009), whereas improper urban planning is also one of the influencers of UHI (Sarvestani et al. 2011). LULC is an important component in the UHI study (Díaz and Blackburn 2003) along with LST, soil moisture and evapotranspiration of the surface, which are the leading factors for the high rise in UHI (Becerril-Piña et al. 2016).

Researchers also often utilize remote sensing-derived Normalized Difference Vegetation Index (NDVI) and Normalized Difference Built-up Index (NDBI) to evaluate UHI effectively (Zhang et al., 2022). NDVI is useful for examining the cooling effects of urban green spaces. Higher NDVI values indicate more vegetation, which typically corresponds to lower LST values, suggesting vegetation's role in mitigating UHI. Li et al. (2011) found that

urban areas with higher NDVI values generally exhibit reduced surface temperatures, underscoring the importance of green infrastructure in urban planning. NDBI is specifically designed to highlight built-up areas by using remote sensing data, making it a more suitable and efficient method for identifying urban features compared to Land Use/Land Cover (LULC) classification methods. LULC maps, while useful, may not always provide the same level of precision in distinguishing between different types of urban and non-urban land covers. For instance, Chen et al. (2023) demonstrated that using NDBI in UTFVI studies allows for a more detailed and precise analysis of the relationship between built-up areas and temperature variations, enhancing the understanding of how urbanization impacts thermal environments.

The effect of UHI can also be quantitatively computed using the Urban Thermal Field Variance Index (UTFVI). UTFVI provides a comprehensive view of the thermal conditions in urban areas by considering both temperature and vegetation cover. This index helps identify areas with high thermal stress, which are critical for targeting UHI mitigation efforts. Zhang et al. (2006) demonstrated that UTFVI could effectively assess thermal comfort levels in urban parks, highlighting areas needing intervention to improve urban living conditions. The results of UTFVI values are divided into six categories (Excellent, Good, Normal, Bad, Worse, Worst), and each category corresponds to a fixed Ecological Evaluation Index (EEI), which was used for evaluating thermal comfort (Ahmed, 2018). A previous study by Naim and Kafy (2021) assessed the UTFVI and defined the relationship between land cover and surface temperature in Chattogram City to identify the temporal changes of intensity of the UHI. Therefore, the combination of LST, UTFVI and NDVI is essential for identifying and analyzing heat patterns across urban landscapes, which are critical for understanding the intensity and distribution of UHI. Thus, the present case study for Tiruppur Corporation considered these indices in order to model the spatial distributions of UHI and thermal comfort. The study would help to improve future urban planning, including the implementation of green city technologies.

Study area

Tiruppur is considered to be the most urbanized developing district of Tamil Nadu state in recent times. Tiruppur corporation is the fifth most agglomerated urban Centre of Tamil Nadu based on census of India 2011. It is located at 10˚14' N to 77˚27' E and 11˚20' N and 77˚56' E on the banks of the Noyyal River (figure 1). It covers an area of 160 sq. km and is situated 450 kilometres southwest of the state capital Chennai and about 50 kilometres east of Coimbatore. The climate of Tiruppur is tropical, with the mean maximum and minimum temperatures varying between 35°C and 22 °C (95 to 72 °F). The total population of the corporation as of the 2011 census was 8,77,778 individuals. Tiruppur has experienced significant fluctuations in rainfall over the years. A study by Kaviya and Elango (2021) indicates that the region has seen variable monsoonal patterns, with periods of drought alternating with years of intense rainfall. Specifically, annual rainfall has ranged from 400 mm in drought years to over 1200 mm during years of good rainfall.

These fluctuations have had substantial impacts on water resources, agricultural productivity, and urban water supply. Temperature trends in Tiruppur show a clear upward trajectory over the past few decades. According to a recent study by Gnanasekaran et al. (2022), there has been a marked increase in both average maximum and minimum temperatures. The study reports that the average maximum temperature has increased by 1.5°C, and the average minimum temperature has increased by 1.2°C over the past 30 years. This rise in temperature has been attributed to global warming and increased urbanization, which exacerbate the urban heat island effect. Over the past few decades, the city has transformed into a major centre for textile manufacturing and export. The study by Balaji and Sundararajan (2020) highlights the rapid expansion of textile units, driven by both domestic and international demand.

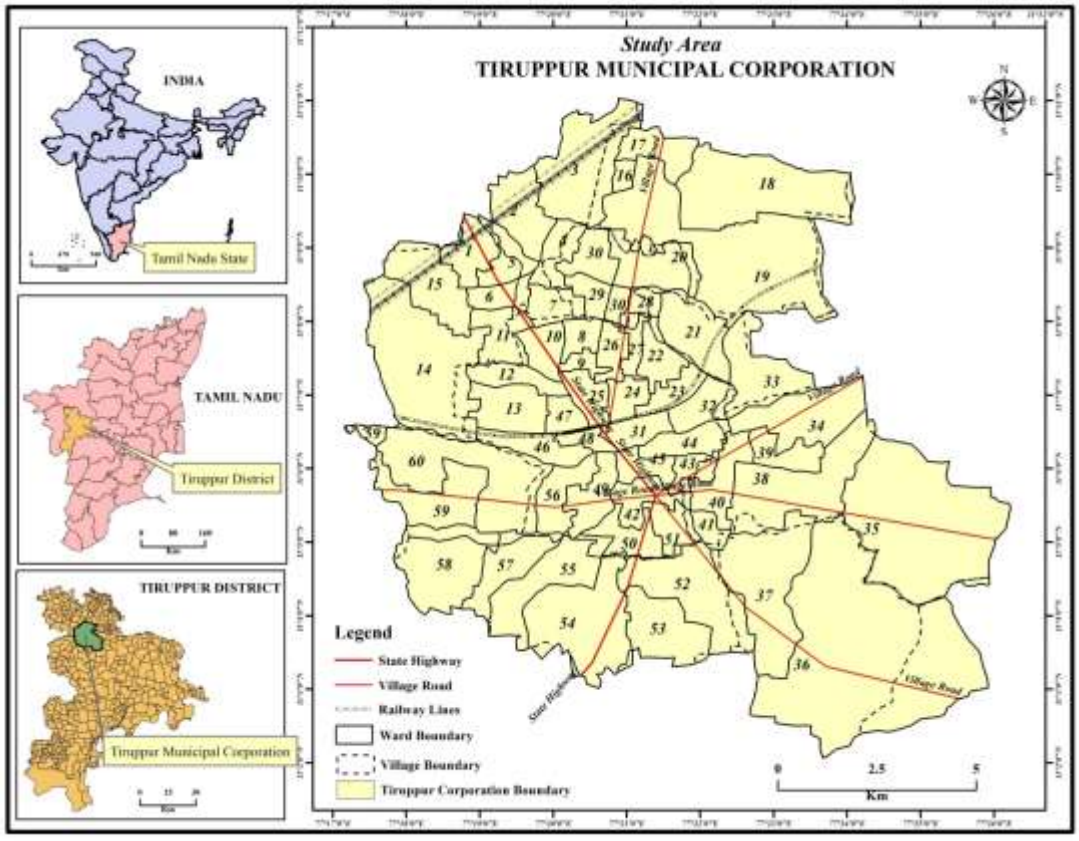

Figure 1: Location map of the Study Area with corporation and ward boundaries

Data Used and Methodology

The present study focused on modelling the Urban Heat Island of Tiruppur Municipal Corporation (TMC) using the Urban Thermal Field Variance Index for the years 1991, 2001, 2011 and 2021. The satellite images of Landsat 5 and 8 have been utilised from the Google Earth Engine Catalog -for computing UTFVI. Computation of UTFVI

requires Normalised Difference Vegetation Index (NDVI) and Land Surface Temperature (LST), as shown in Figure 2. NDVI is calculated by utilising the red and near-infrared (NIR) bands of Landsat data. Then, LST is calculated from the thermal bands of Landsat data through the mono-window algorithm (Li et al. 2022). The formulas for the calculation of LST and UTFVI are discussed below. The mean value of each season is considered for analysis and mapping.

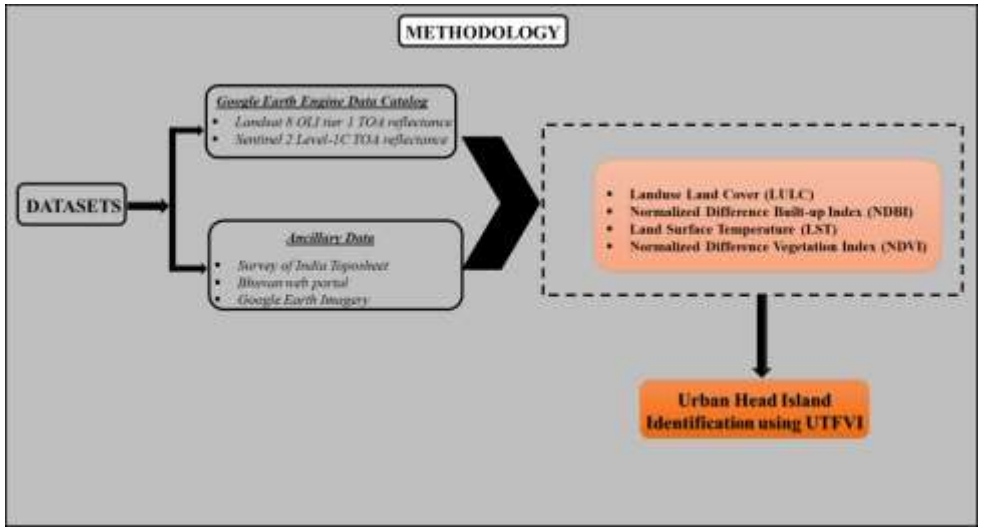

Figure 2: Methodological Framework

The radiance of the Landsat 5 image is calculated using the following equation (1):

$$L\lambda = LMIN\lambda + [(LMAX\lambda - LMIN\lambda) / QCALMAX] \times QCAL \quad \text{.....(1)}$$

Where, LMINλ = spectral radiance scales to QCALMIN (1.238), LMAXλ = spectral radiance scales to QCALMAX (15.303), QCALMIN = the minimum quantized calibrated pixel value (typically 1), QCALMAX = the maximum quantized calibrated pixel value (typically 255), QCAL = digital number.

The effective at-sensor brightness temperature (BT), also known as black body temperature, is obtained from the spectral radiance using Plank's inverse function (2).

$$BT = K2 / \ln (K1/L\lambda + 1) \quad \text{.....(2)}$$

Where, BT=Brightness temperature in Celsius, K1 (607.76) and K 2 = band-specific thermal conversion constant (Landsat 5 TM 1260.56), Lλ = Top of Atmospheric spectral radiance.

The final Land Surface Temperature (LST) is estimated by the equation (3),

$$BT = K2 / \ln (K1/L\lambda + 1) - 273.15 \quad \text{.....(3)}$$

Land Surface Temperature for Landsat 8 TIRS Sensor is calculated by conversion of DN values to at-sensor Radiance

$$L_{sensor\lambda} = M_\lambda * DN + A_\lambda \quad (4)$$

where, $L_{sensor\lambda}$ = spectral radiance (W/ (m2 * sr * μm)), M_λ = radiance multiplicative scaling factor for Band 10 = 0.0003342 (retrieved from Landsat 8 metadata file), A_λ = radiance additive scaling factor for Band 10 = 0.1 (retrieved from Landsat 8 metadata file) and DN = digital number.

Brightness temperature (TB) can be computed using the pre-launched calibration constants (K1 and K2) as expressed in the equation. Brightness temperature is the microwave radiation radiance travelling upward from the top of Earth's atmosphere. The calibration process has been done to convert thermal DN values of thermal bands to TB. Where, K_1= 774.8853, K_2 = 1321.0789 are retrieved from Landsat 8 metadata file.

$$T_B = \frac{K_2}{Ln(\frac{K_1}{L_\lambda}+1)} - 273.15 \quad (5)$$

The land surface emissivity values are obtained using equation (6).

$$\varepsilon = m.P_v + n \quad (6)$$

where, m = 0.004 and n = 0.986. PV is the proportion of vegetation extracted using equations 7 and 8.

$$P_v = \left[\frac{NDVI - NDVI_{min}}{NDVI_{max} - NDVI_{min}}\right]^2 \quad (7)$$

$$NDVI = \frac{NIR - RED}{NIR + RED} \quad (8)$$

where, NDVI is the normalized difference vegetation index. NDVI min and NDVI max are the minimum and maximum values of the NDVI, respectively. NDVI produces values in the range of -0.1 to +0.1, where vegetation areas will typically have values greater than zero, and the negative values indicate non-vegetative areas like urban, water, barren, ice, snow or clouds.

Emissivity corrected LST

Brightness temperatures assume that the Earth is a blackbody, which it is not, and this can lead to errors in surface temperature. In order to minimize these errors, emissivity correction is important and is done to retrieve the LST using an equation (9)

$$LST = {}^{T_B}\Big/_{1 + \left(\lambda * \frac{T_B}{C_2}\right) * Ln(\varepsilon)} \quad (9)$$

where LST is the Land surface temperature (in degree Celsius ˚C), TB is the Brightness temperature, λ =10.8 μm is the effective wavelength of Landsat 8 OLI images, e is the land surface emissivity, which is equal to 1.438 x 10-2 mK in which σ is the Boltzmann constant (1.38 x 10-23 J/K), h is the Plank's constant (6.623 x 10-34 Js) and c is the velocity of light (3 x 108 m/s).

Land Use / Land Cover (LULC)

The LULC were prepared by utilizing the supervised classification algorithm of Support Vector Machine (SVM). SVM is very effective for LULC classification due to their high accuracy, ability to handle non-linear relationships through kernel functions, and robustness to overfitting. Recent research by Maxwell et al. (2023) highlights SVM's effectiveness in producing reliable and precise LULC maps compared to other machine-learning algorithms. SVM's adaptability to high-dimensional data and resistance to outliers make it an excellent choice for remote sensing applications. In this study, the accuracy assessment was done through the Confusion Matrix, and the overall accuracy was above 85% for all the years.

Urban Thermal Field Variance Index (UTFVI)

The UTFVI was estimated using equation (10) and subsequently was classified into six ecological evaluation indices (EEI) and urban heat Island phenomena, as shown in Table 1, which were used for evaluating the level of thermal comfort (Liu and Zhang 2011).

$$UTFVI = \frac{T_s - T_{mean}}{T_{mean}} \quad \text{.....(10)}$$

where TS is the LST (˚C) and Tmean is the mean LST (˚C).

Table 1. Threshold values of Urban Thermal Field Variance Index, Urban Heat Island Class and Ecological Evaluation Index

Urban Thermal Field Variance Index (UTFVI)	Urban Heat Island (UHI)	Ecological Evaluation Index
<0	None	Excellent
0.000 – 0.005	Weak	Good
0.005 – 0.010	Middle	Normal
0.010 – 0.015	Strong	Bad
0.015 – 0.020	Stronger	Worse
>0.020	Strongest	Worst

Results and Discussion

The factors such as the LULC, NDVI, LST, NDBI and UTFVI are computed to identify the UHI of the TMC and its surroundings. All the results are segmented with six rings of each 2km in order to analyse the surrounding scenario. The buffer rings are

selected based on the centroid of the study area boundary. The results and discussion of the following factors are given below.

Landuse Land Cover (LULC)

The LULC for the study region has been classified based on the NRSC level 1 classification, which includes water bodies, built-up, vegetation, agricultural land, and barren land for the temporal years 1991, 2001, 2011, and 2021. In 1991, the built-up of ring 1 was about 54.31% which is a constant decrease from ring 1 to ring 6 and is about 3.59 %. Similarly, the water bodies also constantly decrease from ring 1(4.60%) to ring 6 (0.90%). Then, the vegetation class is very low in ring 1, covering only 8.73% of the area, which has a sudden increase of 18.82% in ring 2, and its proportion increases to 20.44% in ring 6. Further, the barren and agricultural land has uneven distributions of variation between rings 1 and 6, as shown in Figure 3, in which the agricultural land shows a greater variation from 13.47% to 56.69% between rings 1 and 6.

In 2001, the built-up of ring 1 increased from 54.31 % to 82.62 % and in ring 6, 3.59% to 4.27 compared with the previous decade. The number of water bodies has also been reduced compared with the 1991 result. The vegetation also decreased from 8.73% to 2.37% in ring 1 and 20.44% to 11.87 % in ring 6. The barren land and agricultural land have a greater variation where the barren land decreased from 18.89% to 3.26 % in ring 1 and increased from 18.38 % to 19.41% in ring 6; in the case of agriculture, it decreased from 13.47% to 9.65 % in ring 1 and increased from 56.69% to 63.74% in ring 6 between the years of 1991 and 2001.

Compared with the year 2001, the built-up was increased in ring 1 from 82.62% to 84.25% and in ring 6 it increased to 4.27% to 5.43% in 2011. The water bodies were also reduced to 0.04% in 2011 compared to previous temporal years. The vegetation decreased from 2.37% to 1.02% in ring 1 and 11.87 % to 8.16% in ring 6 in 2011. The barren land has decreased from 3.26% to 2.38% in ring 1 and 19.41% to 15.37% in ring 6. However, in Agriculture it has increased from 9.65% to 12.30% in ring 1 and 63.74% to 70.93% in ring 6 in 2011.

In 2021, the built-up has slightly increased from 84.25% to 86.23% in ring 1 and 5.43% to 9.80% in ring 6 compared to 2011. In ring 1, water bodies are 0.04% in 2011 and 2021; in ring 6, it has increased from 0.10% to 1.20% in 2021. The vegetation has been increased from 1.02% to 8.17% in ring 1 and 8.16% to 16.16% in ring 6. The barren land has increased from 2.38% to 3.82% in ring 1 and 15.37% to 44.67% in ring 6 in 2021. Agriculture has been reduced from 12.30% to 1.74% in ring 1 and ring 6, and it has reduced to 70.93% to 28.16% in 2021.

Normalized Difference Vegetation Index (NDVI)

The values of NDVI are categorised into five classes as very low (<0.2), low (0.2 – 0.3), moderate (0.3 – 0.4), high (0.4 – 0.5) and very high (> 0.5) for all the four years of 1991, 2001, 2011 and 2021 (figure 4). It is interpreted from the results that the spatial distribution of the NDVI class is very low in ring 1 and is gradually increasing in the consequent rings towards ring 6 in almost all four years of 1991, 2001, 2011 and 2021. In ring 1 of 1991, the mean value of NDVI is marked as 0.253, which has decreased across the years 2001, 2011 and 2021 to 0.181, 0.176 and 0.174, respectively. Similarly, in ring 3, there was a marked decrease in mean values from 0.343 in 1991 to 0.207 in 2021. Further, in the 6th ring of 1991, it was noticed as 0.389 and decreased to 0.331 (2001), 0.257 (2011) and 0.238 (2021).

In ring 1 of 2001, the mean value of NDVI is marked as 0.181, which decreased across the years of 2011 and 2021 to 0.176 and 0.174, respectively. Similarly, in ring 4, there was a marked increase in mean values from 0.305 in 2001 to 0.211 in 2021. The following 5th ring gradually decreased in the mean values of 0.251 in 2011. Additionally, in the 6th ring of 2001, it was noticed as 0.331 and increased to 0.257 (2011) and 0.238 (2021).

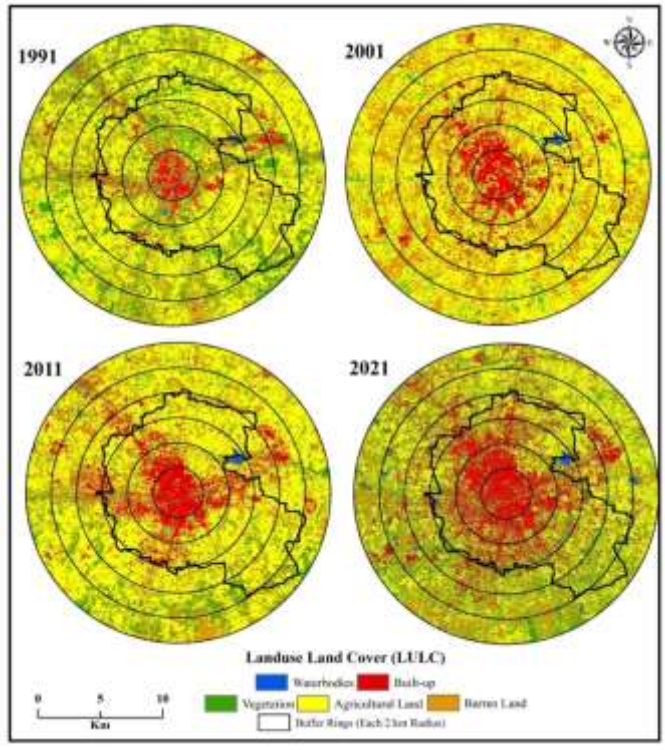

Figure 3: Spatial Distribution of Landuse and Land cover

In 2011, there was a decrease in NDVI values compared to 2001 across all rings, indicating potential changes in vegetation density over the decade. Despite this decrease, the general pattern of higher NDVI values in the inner rings persists, with ring 6 maintaining the highest value at 0.257. Similarly, in ring 1, there was also a marked increase in mean values from 0.176 in 2011 to 0.174 in 2021. The 3rd ring gradually decreased in the mean values of 0.217 in 2011. Further, in the 6th ring of 2011, it was noticed as 0.257 and decreased to 0.238 (2021). By 2021, NDVI values will continue to decline compared to 1991, 2001, and 2011. This decline suggests potential environmental changes affecting vegetation health. However, the inner rings consistently show lower NDVI values compared to the outer rings across all years. Ring 6 maintains the highest NDVI value in 2021, with lower values in previous years, such as ring 1 performing the lowest value in 2021 (0.174). In this study area, NDVI values significantly changed from 2011 to 2021, and the main reason for the growth of urbanization and increasing human activities.

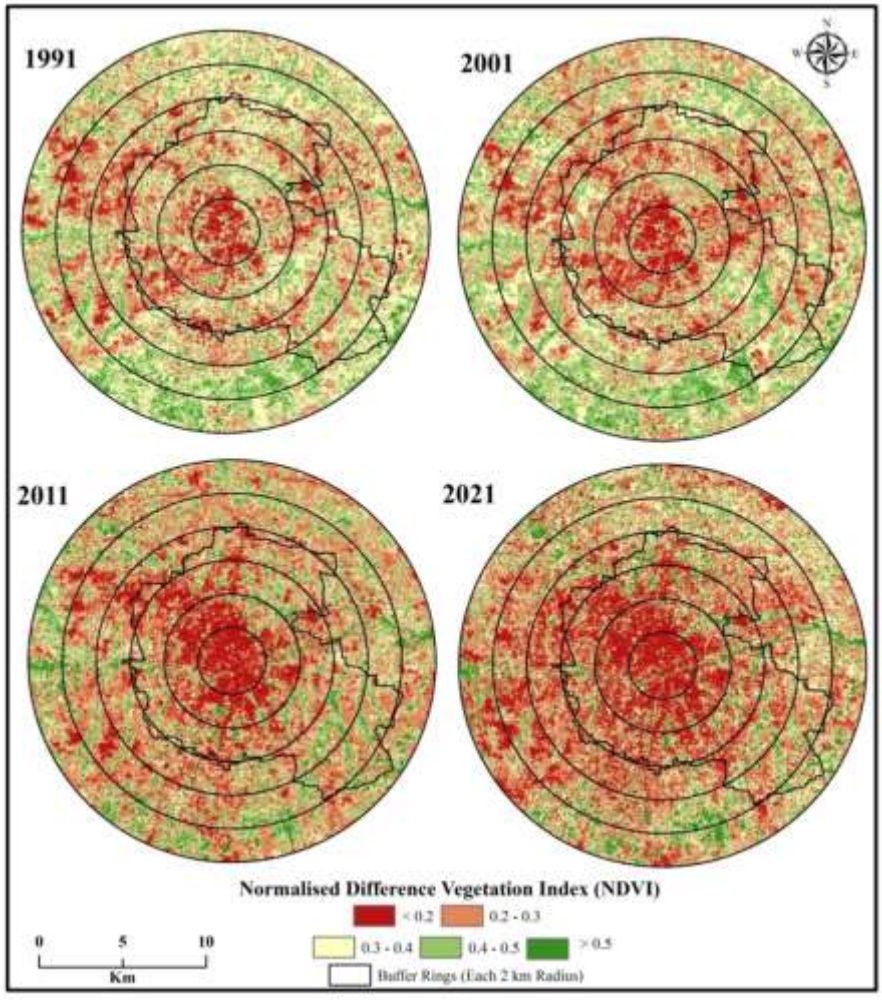

Figure 4: Spatial Distribution of Normalized Difference Vegetation Index

Land Surface Temperature (LST)

In 1991, the Land Surface Temperature (LST) values across all rings remained relatively stable over the decade, with minor anomalies observed. Rings 1 to 3 showed LST values ranging from 39.08 to 40.22, indicating a consistent temperature increase. Rings 4 to 6 also exhibited stable LST values, with temperatures ranging from 40.20 to 40.37 (figure 5).

By 2001, the LST values remained largely consistent compared to 1991, with minimal changes observed across all rings. Rings 1 to 4 maintained LST values of 40.22 to 40.27, indicating stable temperature patterns similar to the previous decade. Similarly, Rings 5 and 6 exhibited minor changes in LST values, ranging from 40.20 to 40.37. Here, in the year 2001, the outer region exhibited high LST values due to the distribution of a high amount of barren land without vegetation, which exhibits a larger amount of surface temperature than the core built-up areas.

In 2011, there was a noticeable increase in LST values across all rings compared to previous years. Rings 1 to 3 experienced a significant temperature rise, with LST values ranging from 45.91 to 43.33, indicating warmer conditions. Similarly, Rings 4 to 6 showed LST values ranging from 40.58 to 40.34. As a result, increasing temperatures across the study area in 2011 are potentially indicative of environmental changes or urban growth effects. By 2021, there was a slight decrease in LST values compared to 2011, although temperatures remained relatively high across all rings. Rings 2 to 4 exhibited LST values ranging from 42.19 to 41.21, indicating warm conditions. Similarly, Rings 5 to 6 maintained temperatures ranging from 39.68 to 40.31. Despite the slight decrease, the data suggests continued warmth across the study area in 2021, showing the processes of urbanization and some ongoing factors influence the surface temperature.

Normalized Difference Built-up Index (NDBI)

The purpose of the Normalized Difference Built-up Index (NDBI) in this study is to identify the Urban Thermal Field Variance Index (UTFVI) accurately to quantify and map urban built-up areas, which are critical in understanding the urban heat island (UHI) effect. The NDBI is calculated for the study region across the years of 1991, 2001, 2011 and 2021. These results are compared with Google Earth, and the threshold value for the built-up regions is identified as 0.36, by which the NDBI values are classified into two classes: built-up and non–built-up class. The results clearly illustrate the spatial distribution and development of built-up across the rings in each year and also the development across the temporal years (figure 6).

In 1991, the intensity of built-up was only marked in ring 1 and ring 2, whereas in other rings the distribution of built-up was very dispersed and scattered. However, during the year 2001, the concentration of built-up extended towards ring 3 and also the intensity in rings 1 and 2 increased when compared to the previous decade. The condition in 2011

is almost similar to that of the distribution in 2001, since the extension of built-up concentration is absent in the fourth ring; instead, the intensity of built-up is increased in the rings 1, 2, and 3. Further, in 2021, a larger increase of built-up was noticed in all the rings, and the intensity of the built-up was extended to ring 4 of the study region. In addition, it is noticed that the intensity of built-up has attained its maximum extent in the rings 1 and 2.

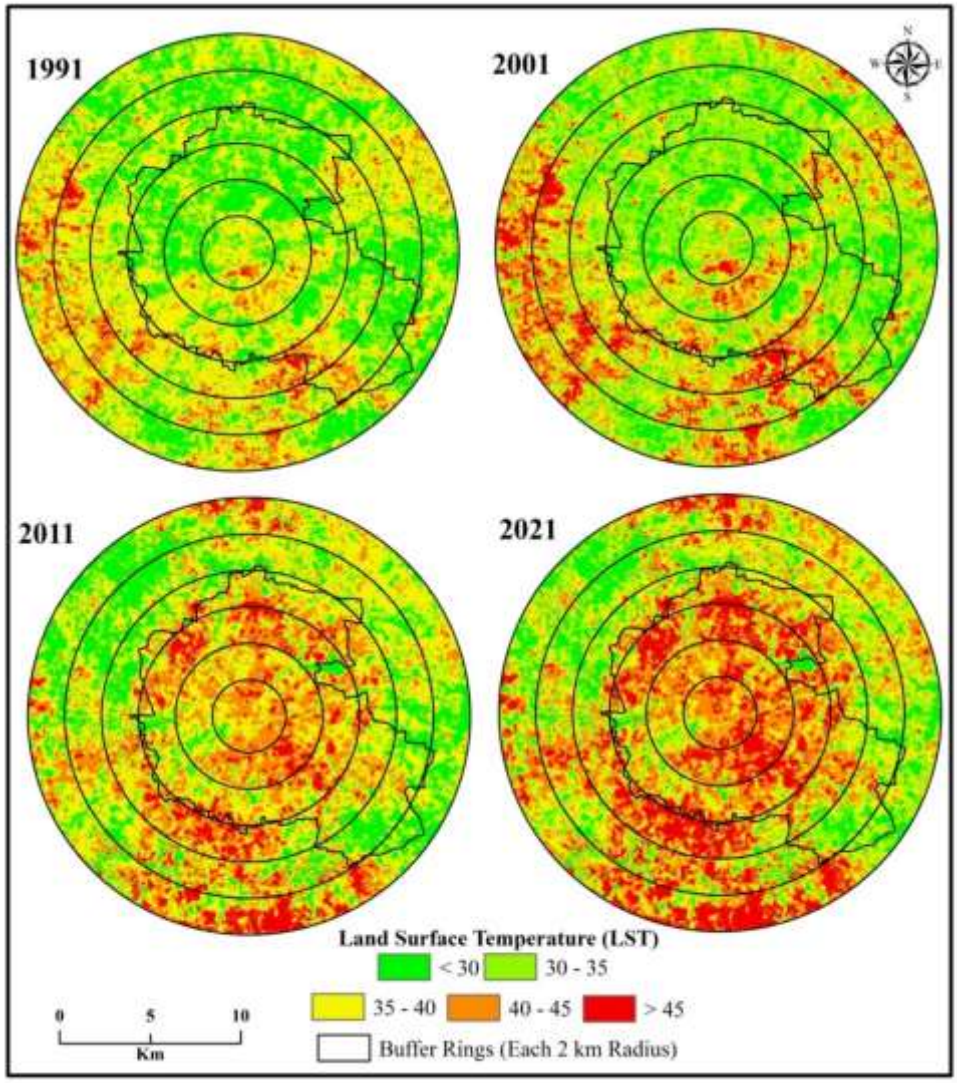

Figure 5: Spatial Distribution of Land Surface Temperature

Urban Thermal Field Variance Index (UTFVI)

The urban thermal field variance index is basically a conceptual factor based on surface temperature, which also defines urban heat islands. The Urban thermal field is

classified into six classes based on the Urban Heat Island aspect such as none (<0), weak (0.000 -0.005), middle (0.005-0.010), strong (0.010-0.015), stronger (0.015-0.020), strongest (>0.020) for 1991, 2001, 2011, and 2021. As per the results of UTFVI, the temperature gradually increases from 1991 to 2021 (figure 7).

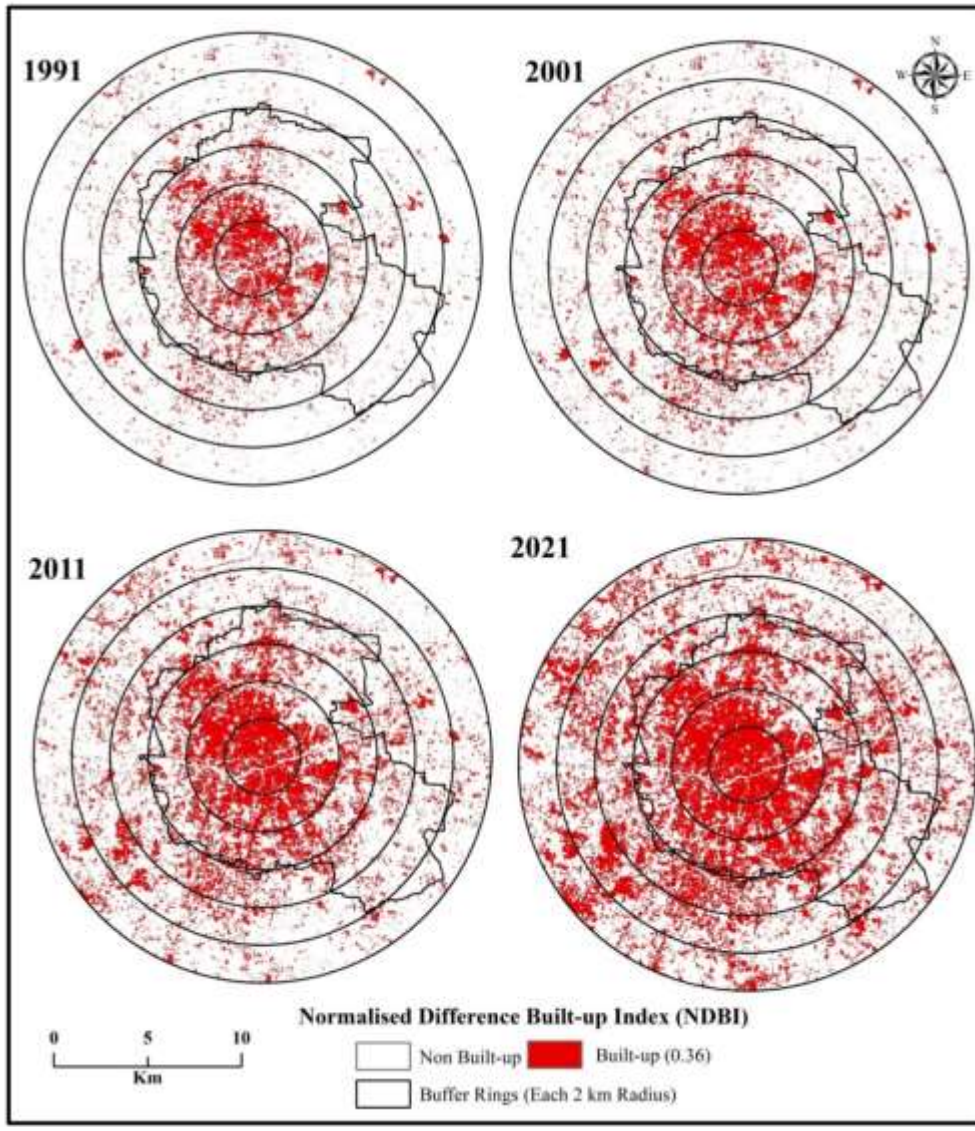

Figure 6: Spatial Distribution of Normalized Difference Built-up Index

In 1991, the structural distribution of thermal variance was relatively low compared to the respective years. In ring 1 there is only a distribution of strong and stronger classes where it is changed to a high distribution of stronger and a low distribution of strong classes

in the same ring during the year 2001. This condition is even more different in 2011, when some of the stronger UHI conditions are changed to the strongest UHI conditions. Thus, in the year 2021, most of the parts of ring 1 fall under the strongest UHI condition. This is the similar condition in the ring 2 as well in all the observed years. However, in ring 3, during 1991, there is a maximum distribution of strong UHI conditions along with the distribution of none, weak and middle class. However, this distribution has tremendously changed across the years 2001, 2011 and 2021 as the none-to-middle UHI class is reduced, and most of the portions of ring 3 are increased with the strong to strongest class condition. Moreover, as mentioned in the LST, here in the year 2001, the UTFVI value is higher in the outer ring than in the core rings due to the abundant distribution of barren land in the outer rings. It is noticed from the result of UTFVI that the Tiruppur Municipal Corporation is highly affected by the heat stress that is from ring 1 to ring 4 of 2021 is falls under the stronger and strongest UHI class. In addition, the northwest portion of the study region is also affected by the strong to strongest UHI condition in all four years.

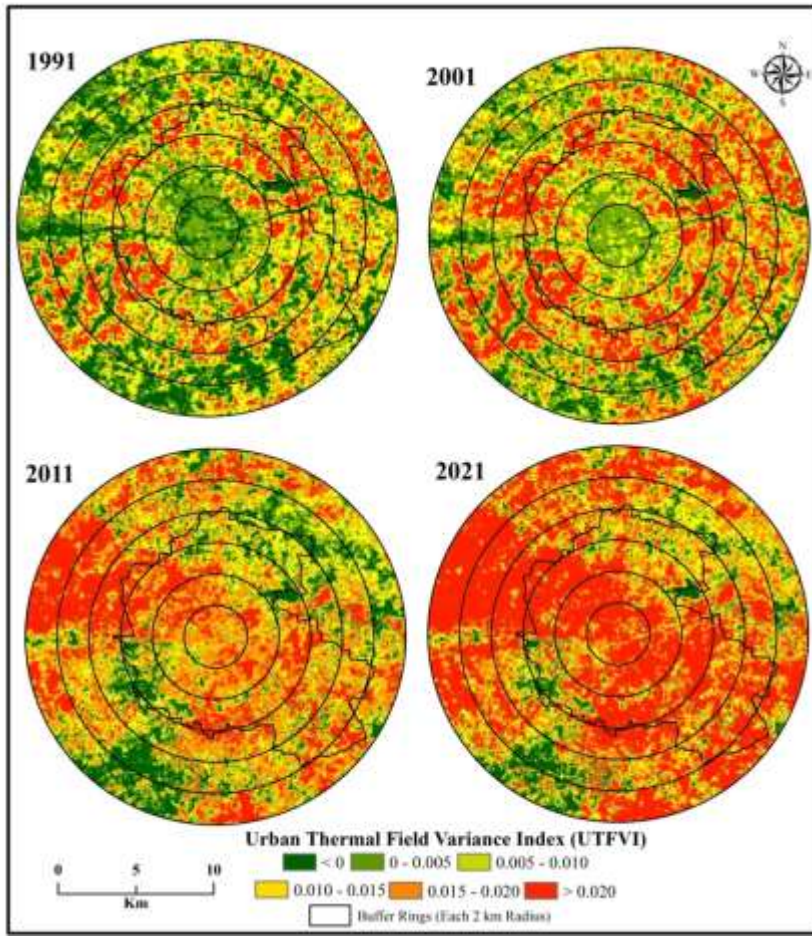

Figure 7: Spatial Distribution of Urban Thermal Field Variance Index

Identifying the trend of UHI is very helpful in designing appropriate adaptation methods for sustainable urban growth. A previous study by Moisa et al. (2022) found that the urban thermal environment is highly influenced by changes in LULC. In this present study, the temporal changes of the LULC along with the LST, NDVI, NDBI, and UTFVI were identified to determine the influence of urbanization on UHI phenomena in the study area. A similar study by Moisa and Gemeda (2022) assesses the urban thermal field variance index and thermal comfort level of Addis Ababa metropolitan city, Ethiopia. Their study categorised them into six zones to identify the UHI.

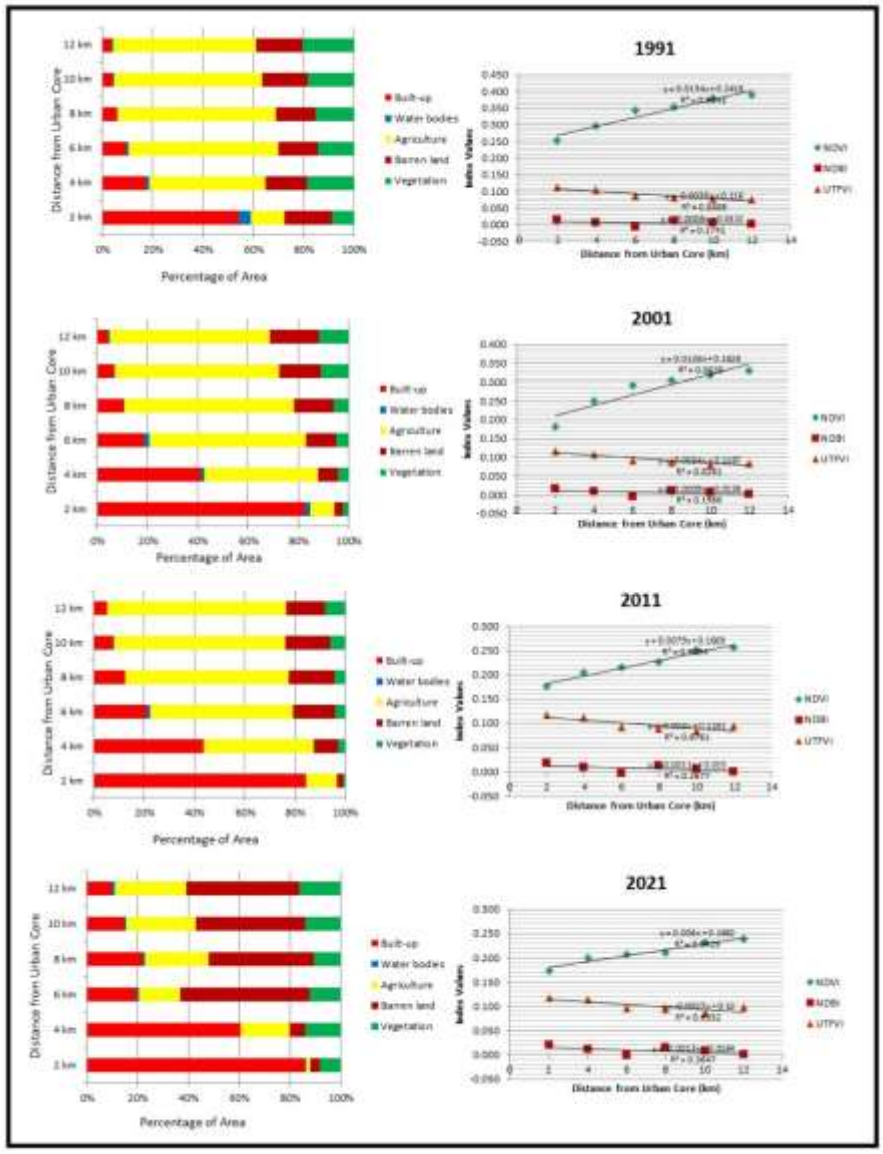

Figure 8: Graphical Representation of land use / Land cover, NDVI, NDBI and UTFVI

In the present study, during 1991, the structural distribution of thermal variance was relatively low compared to the recent years. In ring 1, there is only a distribution of strong classes, which changed to stronger classes in the year 2001. This condition became even more intense in 2011, when some of the stronger UHI conditions were changed to the strongest UHI conditions. Thus, in the year 2021, most of the parts of ring 1 fall under the strongest UHI condition. This condition is supported by the other factors where the NDVI values are very low, indicating very low vegetation; the LST values are high, indicating very high temperature; and the NDBI values are also very high, indicating high intensity of built-up distribution. The result of LULC also supports the UTFVI result with the higher distribution of built-up in the same ring. Accordingly, the strong to strongest classes are increasing exponentially during these years (1991 to 2021) and are mostly concentrated over the core in the central rings 1 and 2 and also in the northwestern portions of the study region (rings 4, 5, 6) during the year 2011 and 2021. However, it is observed that during the years 1991 and 2001, the core areas exhibited less LST and UTFVI than the outer rings, which have a high distribution of barren land without vegetation, which poses a higher surface temperature than the built-up (figure 8). This condition is also supported by the higher decrease of vegetation (NDVI), increase of temperature (LST) and the increase of built-up (NDBI and LULC). By identifying the areas most affected by UHI, this research provides a clear spatial understanding of heat distribution within the city. The findings can be leveraged to prioritize cooling measures in the most vulnerable neighbourhoods. Incorporating more green spaces and implementing green roofing and cool roofing technologies can foster a more resilient urban environment in Tiruppur city.

Conclusion

The present study aims to identify the impact of urbanization on the increasing temperature and development of urban heat islands in Tiruppur city. The urban expansion and distribution are inferred by analysing the LULC, NDVI, and NDBI changes from 1991 to 2021 at a decade interval. These spatio-temporal changes were compared with temperature analysis by computing LST and UTFVI. The result infers that the strong to strongest classes are increasing exponentially from 1991 to 2021 and are mainly concentrated over the city core, such as rings 1 and 2, and in the northwestern portions of the study region, in rings 4, 5 and 6. This inference is supported by the decrease of vegetation (NDVI), increase of temperature (LST) and the increase of built-up (NDBI and LULC). Thus, in the near future, this urban heat island will increase enormously to the outer rings and affect all the life forms. The findings of this study offer crucial insights that can significantly aid governance in devising effective strategies to combat urban heat and improve the overall quality of life for residents in TMC. Policymakers can use these insights to enforce stricter regulations on building materials and urban designs that contribute to heat retention, ensuring that resources are allocated efficiently and effectively.

Competing Interests

The authors declare that there are no competing interests.

Acknowledgement

Masilamani Palanisamy is the awardee of ICSSR minor research project (File No. 02/3/SC/2021-22/ICSSR/RP/MN). This paper is largely an outcome of the Research project sponsored by the Indian Council of Social Science Research (ICSSR). However, the responsibility for the facts stated, opinions expressed, and the conclusions drawn is entirely that of the author. The authors would like to thank the Department of Geography (SAP DRS-II, RUSA 2.0) Bharathidasan University for letting to utilize the lab facilities and their support. All authors would like to thank Prof. K. Kumaraswamy and Prof. R. Jegankumar for their support. The authors extend their thanks to Dr. S. Abdul Rahaman, Mr. K. Prakash, Mr. J. Killivalavan and Ms. Thanuja Krishnan R. for their support.

References

1. Abdikan, S., Balik Sanli, F., Sunar, F., & Ehlers, M. (2014). A comparative data-fusion analysis of multi-sensor satellite images. International Journal of Digital Earth, 7(8), 671-687.
2. Ahmed, S. (2018). Assessment of urban heat islands and impact of climate change on socioeconomic over Suez Governorate using remote sensing and GIS techniques. The Egyptian Journal of Remote Sensing and Space Science, 21(1), 15-25.
3. Balaji, P., & Sundararajan, M. (2020). Their study provides insights into the growth of the textile industry in Tiruppur, discussing its economic significance and the factors driving this expansion.
4. Becerril-Piña, R., Díaz-Delgado, C., Mastachi-Loza, C. A., & González-Sosa, E. (2016). Integration of remote sensing techniques for monitoring desertification in Mexico. Human and Ecological Risk Assessment: An International Journal, 22(6), 1323-1340.
5. Bongaarts, J. (2020). United Nations Department of Economic and Social Affairs, Population Division World Family Planning 2020: Highlights, United Nations Publications, 2020. 46 p.
6. Brandsma, T., & Wolters, D. (2012). Measurement and statistical modelling of the urban heat island of the city of Utrecht (the Netherlands). Journal of Applied Meteorology and Climatology, 51(6), 1046-1060.
7. Chen, J., Li, X., Zhao, W., & Wu, J. (2023). Integration of NDBI and other remote sensing indices for comprehensive analysis of urban heat island effects: A case study in Beijing, China. Remote Sensing of Environment, 280, 113247. doi:10.1016/j.rse.2022.113247/
8. Díaz, BM., & Blackburn, GA. (2003). Remote sensing of mangrove biophysical properties: evidence from a laboratory simulation of the possible effects of background variation on spectral vegetation indices. Int JRemote Sens 24:53–73.
9. Gnanasekaran, M., Rajendran, V., & Prakash, K. (2022). The research documents the increasing temperature trends in Tiruppur, exploring the contributing factors and potential impacts on urban life.

10. Gordon, A., Simondson, D., White, M., Moilanen, A., & Bekessy, S. A. (2009). Integrating conservation planning and landuse planning in urban landscapes. Landscape and urban planning, 91(4), 183-194.
11. Kaviya, R., & Elango, L. (2021). This study examines the variability in rainfall patterns in Tiruppur, highlighting the implications of these changes on water resources and urban planning.
12. Kesavan, R., Muthian, M., Sudalaimuthu, K., Sundarsingh, S., & Krishnan, S. (2021). ARIMA modelling for forecasting land surface temperature and determination of urban heat island using remote sensing techniques for Chennai city, India. Arabian Journal of Geosciences, 14(11), 1-14.
13. Li, J., Wang, X., Wang, X., Ma, W., & Zhang, H. (2011). Remote sensing evaluation of urban heat island and its spatial pattern of the Shanghai metropolitan area, China. Ecological Complexity, 8(2), 177-183.
14. Li, X., Zhang, X., Wang, Y., & Liu, Q. (2022). Improved split-window algorithm for land surface temperature retrieval from MODIS data. Remote Sensing of Environment, 265, 112660. https://doi.org/10.1016/j.rse.2021.112660/
15. Liu, L., & Zhang, Y. (2011) Urban heat island analysis using the Landsat TM data and ASTER data: a case study in Hong Kong. Remote Sensing 3(7), 1535–1552. https:// doi. org/ 10. 3390/ rs307 1535 /
16. Maxwell, A. E., Warner, T. A., & Fang, F. (2023). Implementation of support vector machines in remote sensing: Recent advances and applications. Remote Sensing, 15(3), 456-472.
17. Moisa, M. B., & Gemeda, D. O. (2022). Assessment of urban thermal field variance index and thermal comfort level of Addis Ababa metropolitan city, Ethiopia. Heliyon, 8(8).
18. Moisa, M. B., Merga, B. B., & Gemeda, D. O. (2022). Urban heat island dynamics in response to land use land cover change: a case of Jimma city, southwestern Ethiopia. Theoretical and Applied Climatology, 149(1-2), 413-423.
19. Naim, M. N. H., & Kafy, A. A. (2021). Assessment of urban thermal field variance index and defining the relationship between land cover and surface temperature in Chattogram city: a remote sensing and statistical approach. Environmental Challenges, 4, 100107.
20. Padmanaban, R., Bhowmik, A. K., & Cabral, P. (2017). A remote sensing approach to environmental monitoring in a reclaimed mine area. ISPRS international journal of geo-information, 6(12), 401.
21. Prakash., Rajagopal, Jegankumar., & Libina, Rs. (2023). Analysing spatial and geometrical patterns of urbanization using spatial metrics – A case study of Tiruchirappalli urban, India. 10.21203/rs.3.rs-2726357/v1.
22. Ranagalage, M., Estoque, R. C., Handayani, H. H., Zhang, X., Morimoto, T., Tadono, T., & Murayama, Y. (2018). Relation between urban volume and land surface temperature: A comparative study of planned and traditional cities in Japan. Sustainability, 10(7), 2366.

23. Sabet Sarvestani, M., Ab Latif Ibrahim., & Pavlos Kanaroglou. (2011).“Three Decades of Urban Growth in the City of Shiraz, Iran: A Remote Sensing and Geographic Information Systems Application.”. Cities, 28(4), 320-329.
24. Stow, D. A., & Chen, D. M. (2002). Sensitivity of multitemporal NOAA AVHRR data of an urbanizing region to land-use/land-cover changes and misregistration. Remote sensing of Environment, 80(2), 297-307.
25. The World’s Cities in 2016. T. W. C. in 2016—D. B. (ST/ESA/S.A.), Population Department, Department of Economic and Social Affairs, United Nations. 2016.
26. Wang, R., Derdouri, A., & Murayama, Y. (2018). Spatiotemporal simulation of future land use/cover change scenarios in the Tokyo metropolitan area. Sustainability, 10(6), 2056.
27. Weng, Q., Lu, D., & Schubring, J. (2004). Estimation of land surface temperature–vegetation abundance relationship for urban heat island studies. Remote sensing of Environment, 89(4), 467-483.
28. Zhang, H., Wang, Y., & Zhang, Y. (2006). Assessing the thermal field of urban parks using remote sensing data. International Journal of Remote Sensing, 27(19), 4199-4214.
29. Zhao, L., Lee, X., Smith, R. B., & Oleson, K. (2014). Strong contributions of local background climate to urban heat islands. Nature, 511(7508), 216-219.
30. Zhou, B., Erell, E., Hough, I., Rosenblatt, J., Just, A. C., Novack, V., & Kloog, I. (2020). Estimating near-surface air temperature across Israel using a machine learning-based hybrid approach. International Journal of Climatology, 40(14), 6106-6121.
31. United Nations. (2018). World Urbanization Prospects: The 2018 Revision. Department of Economic and Social Affairs, Population Division. Retrieved from https://population.un.org/wup/Publications/.
32. Peng, S., Piao, S., Zeng, Z., Ciais, P., Zhou, L., Li, L. Z. X., Myneni, R. B., Yin, Y., & Zeng, H. (2021). Urban heat island impacts on land surface temperature trends in a rapidly urbanizing region. International Journal of Climatology, 41(3), 1710-1720. doi:10.1002/joc.6915.
33. Xiao, J., Shen, Y., Ge, J., Tateishi, R., Tang, C., Liang, Y., & Huang, Z. (2020). Evaluating urban expansion and land use change in Shijiazhuang, China, using GIS and remote sensing. Remote Sensing, 12(8), 1334. doi:10.3390/rs12081334.
34. Zhang, Y., Balzter, H., Liu, B., Chen, Y., & Zhang, X. (2022). A comprehensive analysis of urban heat island dynamics using multi-sensor remote sensing data: A case study of the Yangtze River Delta, China. Remote Sensing of Environment, 271, 112890. doi:10.1016/j.rse.2021.112890.